

14. HUMAN INFLUENCES ON HEAT-RELATED HEALTH INDICATORS DURING THE 2015 EGYPTIAN HEAT WAVE

DANIEL MITCHELL

A combined modeling and observational assessment of the 2015 heat wave in Egypt found that human discomfort increased due to anthropogenic climate change.

Introduction. In August 2015, northeast Africa and the Middle East experienced a heat wave that caused high levels of human discomfort, even for countries particularly adapted to extreme heat. Reports suggest that more than 90 people died throughout Egypt, with the majority being elderly (*Al Jazeera*, 17 August 2015). In and around Cairo, many of the deaths were blamed on overpopulation and cramped living conditions, notably including prisons and psychiatric centers, a problem that is not necessarily restricted to the developing world (*Huffington Post*, 15 August 2015; Holt 2015). The local health ministry reported that persistently high humidity was at least partially to blame. In the previous year (2014), the region experienced an unprecedented drought (Bergaoui et al. 2015; Barlow and Hoell 2015), and combined with political tensions, the recent heat wave could enhance unrest in the region (Schleussner et al. 2016).

While direct attribution of climate change on mortality is possible (Mitchell et al. 2016a), the required observed mortality data are not easily obtained in this specific region. As such, the attribution study is performed on the wet bulb globe temperature (WBGT), a proxy for human discomfort. Note that Mitchell et al. (2016a) used a different heat stress metric, apparent temperature, because this could be used directly with the health impact assessment (HIA) model they employed. As this study does not use a HIA model, the WBGT is chosen so the study can be contrasted with a recent climate predictions study (Pal and Eltahir 2015). A comparison of the two different heat stress metrics is given in Willett and Sherwood (2012).

Methods. The WBGT is estimated using the following equation (Fischer and Knutti 2012):

$$\text{WBGT} = 0.567T + 0.393e + 3.94$$

The water vapor pressure, $e = f(T, RH)$, can be approximated using a derivation of the Magnus formula (Sonntag 1990; Sippel and Otto 2014), where the terms T and RH are temperature and relative humidity, respectively, and are available from model output and from the Met Office Integrated Data Archive System (MIDAS; Met Office 2012) station data. This study focuses on Egypt as a whole, but a subanalysis is also performed for Cairo (the most populated city in Egypt). A map of the station locations is given in Fig. 14.1a with Cairo marked in red.

Event attribution is performed using the `weather@home` framework, which comprises a global atmosphere-only driving model (HadAM3P; Massey et al. 2015) and a 50-km regional model covering northern Africa and the Middle East (the setup is identical to Bergaoui et al. 2015). Approximately 2000 simulations of 2015 are run using perturbed initial conditions (actual scenario) and compared with ~2000 simulations estimating a naturalized version of 2015 (natural scenario). The natural simulations employ solar and volcanic forcings fixed at 2015 levels with all other forcings set to preindustrial values. However, the actual scenarios employ all forcings at 2015 levels, which include the aforementioned natural forcings as well as greenhouse gases, aerosols, and land use. The model is spun up for 2 years before 2015 to equilibrate long-memory processes in the Earth-atmosphere system. The natural scenario simulations include 10 estimates of possible natural sea surface temperatures (SSTs), which are estimated using coupled ocean-atmosphere models (Schaller et al. 2016). The model simulations are interpolated to each of the different station locations.

Results. The observed WBGT over Egypt (i.e., the average of all stations) is shown by the black line

AFFILIATIONS: MITCHELL—Environmental Change Institute, Oxford University, Oxford, England

DOI:10.1175/BAMS-D-16-0132.1

A supplement to this article is available online (10.1175/BAMS-D-16-0132.2)

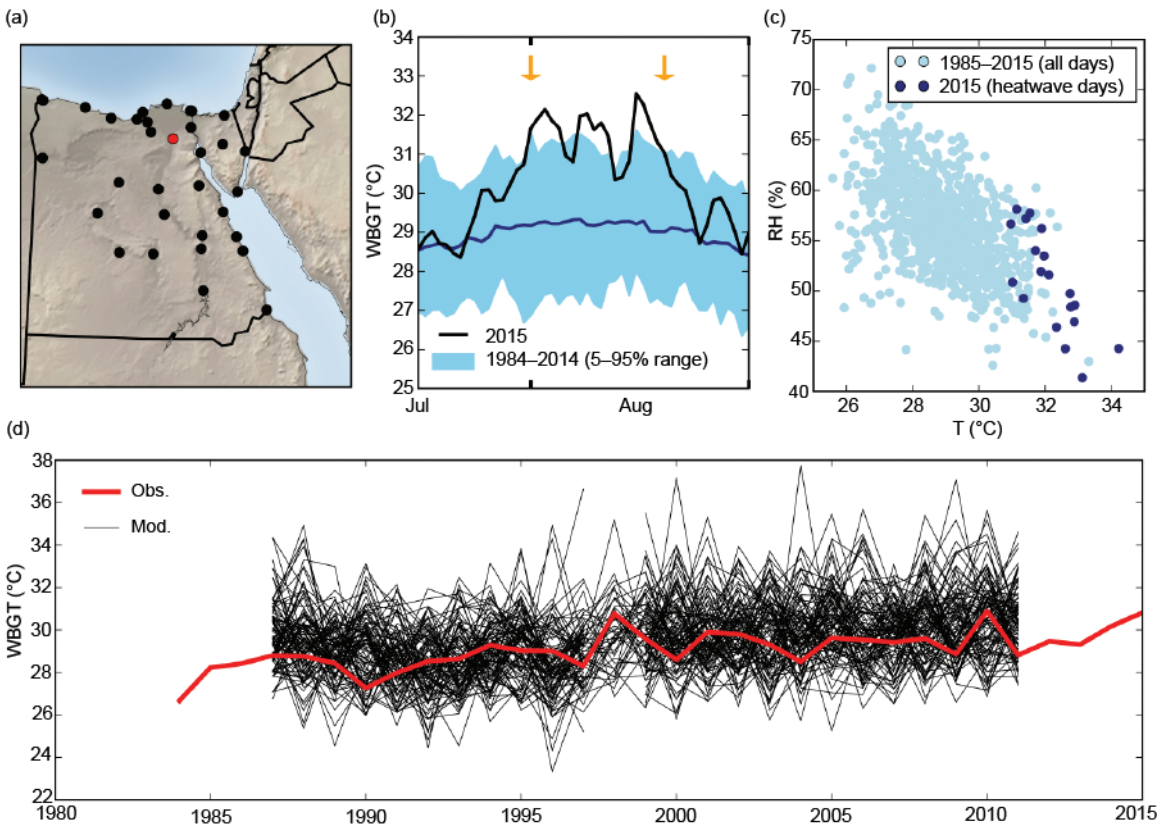


FIG. 14.1. (a) Station locations over Egypt from MIDAS. The red station marks Cairo International Airport. (b) The observed WBGT cycle over Egypt through 15 Jul to 31 Aug. The black line shows 2015; the light blue region is the 5%–95% range covering 1984–2014; and the dark blue line is the climatology. Orange arrows mark the beginning and start of the heat wave (see text). (c) A scatter plot of observed Aug daily temperatures against relative humidity levels (light blue) for all days over the 1984–2015 period, and (dark blue) the days during the 2015 heat wave (first 19 days of Aug). (d) Aug averaged WBGT for (red) observations and (black) individual ensemble members of HadAM3P.

of Fig. 14.1b for 2015. The WBGT in August was a maximum for 2015 and was greater than the 5–95 percentile range of previous years (1984–2014; blue region). Here, the heat wave is defined as starting when the 5–95 percentile in WBGT is exceeded for at least 5 days and ends when the WBGT drops below the 5–95 percentile without exceeding it in the subsequent 5 days. The heat wave event is marked with orange arrows on Fig. 14.1b. While the primary reason for the high WBGT is the high temperatures over this period, the high relative humidity levels (for the given temperature levels) were also important. Around half of the heat wave days had this combination with the other half having approximately average relative humidity levels for the respective temperature levels (Fig. 14.1c).

A reasonable hypothesis would be that this event was made more likely due to human-induced climate change because the observed August WBGT has a significant positive trend over Egypt (Fig. 14.1d,

red line). To test this, model simulations of the 2015 climate over the region are employed. The modeled bias in WBGT is first examined using ~100 ensemble members spanning 1987–2012 (Fig. 14.1c, black lines). This period is chosen because it is the length of time that the required observed SST forcing data are available for the model simulations. The multiensemble mean of the simulations shows a similar trend in WBGT to observations, as can be seen in Fig. 14.1d.

Compared with the observed data, the model performs remarkably well for mean climate with the bias in WBGT over this period being 0.007°C. However, larger biases are observed in the mean temperatures with the model being 1.88°C too warm; and for relative humidity, the model is ~8% too dry. Therefore, the well-simulated mean WBGT in the model is partially due to compensating errors from the temperature and relative humidity being biased in opposing directions (as relevant for heat stress). The variance of daily temperature and WBGT are

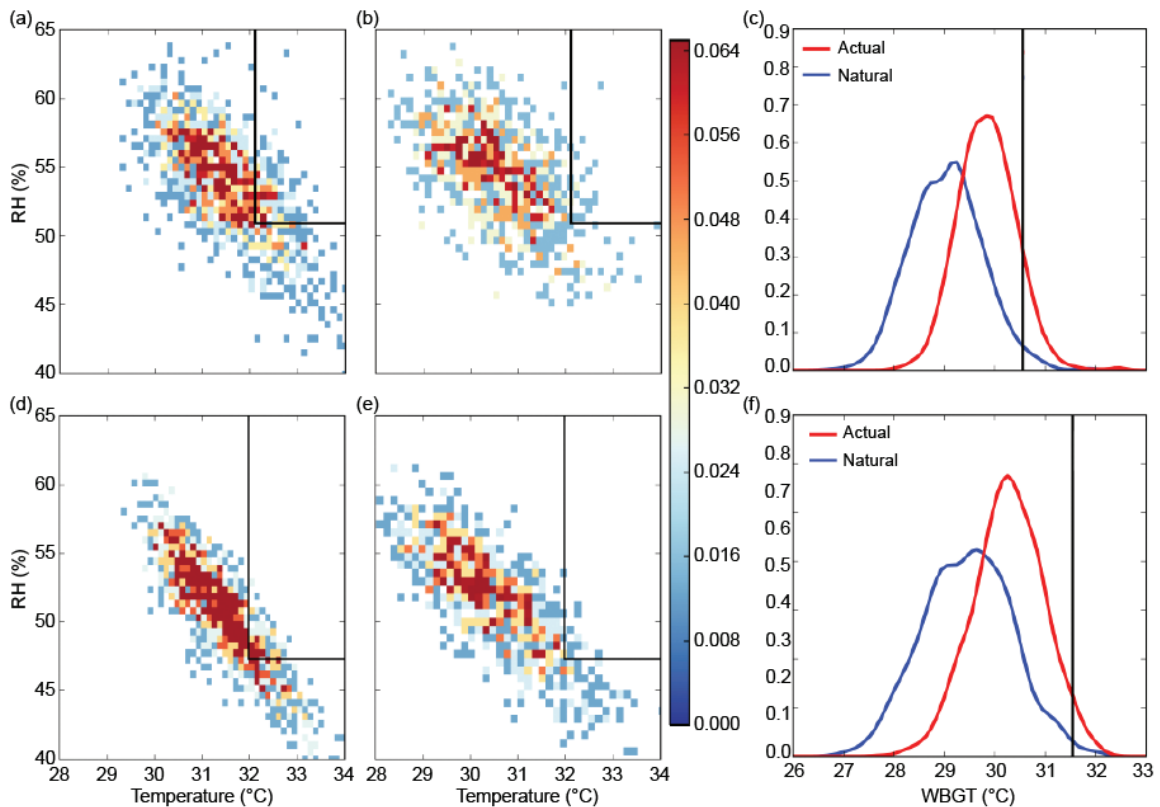


FIG. 14.2. Two-dimensional histograms of 19-day average relative humidity and temperature during Aug for (a),(d) the actual simulations and (b),(e) the natural simulations. (c),(f) One-dimension PDFs of the WBGT for (red) actual and (blue) natural simulations. (a)–(c) For Egypt; (d)–(f) for Cairo. Black lines show the observed value of the variable in question averaged over the first 19 days in Aug 2015. All plots are expressed as a density (i.e., they integrate to 1).

also well reproduced (not shown) although there are large low biases in the variance of modeled relative humidity ($\sigma_{\text{obs}} / \sigma_{\text{mod}} = 1.89$).

Before the event is assessed, the monthly mean and daily variability about the mean for temperature, relative humidity, and WBGT are corrected to match observations at each station location. For temperature, this has been performed in Hempel et al. (2013). Applying their procedure to relative humidity and WBGT also proves to be an adequate bias correction, perhaps, unsurprisingly, as both variables evolve in a similar fashion to temperature. (Note that calculating WBGT from the bias-corrected variables yields almost identical results as calculating WBGT from the raw variables and then bias-correcting. In this assessment, the latter method is used.)

To understand the 19-day event (e.g., Fig. 14.1b) more completely, the coevolution of temperature and relative humidity is contrasted with WBGT. Figure 14.2 shows the 2D histograms of modeled, 19-day averaged, relative humidity, and temperature over Egypt for the actual scenario (Fig. 14.2a) and the

natural scenario (Fig. 14.2b). Figures 14.2d,e show the same but for Cairo only. The black lines show the observed thresholds during the event, and hence model data that fall to the upper-right of these thresholds are more extreme than the observed event. It is clear that more model data exceed the observed threshold in the actual scenario than in the natural. This is true for Egypt as a whole, and specifically for Cairo, and confirms the hypothesis that human-induced climate change has made this event more likely.

Performing the same comparison on the WBGT (Figs. 14.2c,f for Egypt and Cairo, respectively) supports this conclusion. To quantify the level of anthropogenic contribution to the event, the fraction of attributable risk (FAR) is used. This is defined, as in Allen (2003) as $1 - (P_{\text{Nat}} / P_{\text{Act}})$, where P_{Nat} is the probability of exceeding the event in the natural scenario, and P_{Act} is the probability of exceeding the event in the actual scenario.

Over Egypt and Cairo, the FAR values (with 2 sigma errors) in WBGT are calculated as $0.69 (\pm 0.17)$ and $0.67 (\pm 0.07)$, respectively. (Note that if a shorter

averaging period is used, such as 7-day averages, the FAR values are similar for Egypt as a whole, although decrease for Cairo.) While the heat wave center of action was in the south of Egypt (e.g., Haaretz 2015), Cairo (in the north) experienced slightly higher temperatures due to the urban heat island effect (e.g., Heaviside et al. 2015). Luckily, like Cairo, most of Egypt's population resides in the north, with 9 out of 10 of the largest cities (by population) being located there. Had the heat wave been more focused over the north, the death toll could have been far higher.

Conclusions and discussions. In this study, an analysis of heat stress was undertaken for the 2015 Egyptian heat wave. It was found that over Egypt the event was made 69% (\pm 17%) more likely due to anthropogenic climate change, and this was a similar value of 67% (\pm 7%) when only Cairo was considered. The principal driver of human discomfort was high temperature, but relatively high humidity levels for those given temperatures also played a role for around half of the heat wave. It is noted that the daily variance of relative humidity is bias-low in this region. This is especially relevant for the developing regions of the world, as an increased exceedance of critical thresholds (such as the temperature at which the human body can still transfer heat to the surrounding) will be among the most important impacts felt for society under climate change (Pal and Eltahir 2015). This is especially true for high-mitigation scenarios, such as those presented in the 2015 Paris Agreement, because impacts on society will be largely felt through changes in extremes (Mitchell et al. 2016b).

While assessing human health under climate change is of particular importance in this region, it also presents unique challenges. This analysis focuses only on a physical heat stress measure of human discomfort and does not take into account social aspects (e.g., Klinenberg 2002). To do this, a full epidemiological analysis is needed in the first instance (as in Mitchell et al. 2016a). However, while in the context of Africa, meteorological data over Egypt are surprisingly abundant, reliable, and freely available, epidemiological data (such as all-cause mortality) are not. Nevertheless, this study represents a step in understanding health impacts of climate change in the region, and it is hoped that this study and others like it will prompt local governments to make national-level health data more widely available to the outside community.

ACKNOWLEDGEMENTS. Mitchell is funded under the ACE Africa project. I would like to thank all of the volunteers who have donated their computing time to climateprediction.net and weather@home. Also, thanks to the Oxford e-Research Centre and Met Office Hadley Centre PRECIS teams for their technical and scientific support in the development and application of weather@home.

REFERENCES

- Allen, M., 2003: Liability for climate change. *Nature*, **421**, 891–892.
- Barlow, M., and A. Hoell, 2015: Drought in the Middle East and central-southwest Asia during winter 2013/14 [in “Explaining Extreme Events of 2014 from a Climate Perspective”]. *Bull. Amer. Meteor. Soc.*, **96** (12), S71–S76, doi:10.1175/BAMS-D-15-00127.1.
- Bergaoui, K., D. Mitchell, R. Zaaboul, R. McDonnell, F. Otto, and M. Allen, 2015: The contribution of human-induced climate change to the drought of 2014 in the southern Levant region [in “Explaining Extreme Events of 2014 from a Climate Perspective”]. *Bull. Amer. Meteor. Soc.*, **96** (12), S66–S70, doi:10.1175/BAMS-D-15-00129.1.
- Fischer, E. M., and R. Knutti, 2012: Robust projections of combined humidity and temperature extremes. *Nat. Climate Change*, **3**, 126–130, doi:10.1038/nclimate1682.
- Haaretz, 2015: Death toll in Egypt heatwave rises to 106. *Haaretz [online]*, 18 August 2015. [Available online at www.haaretz.com/middle-east-news/1.671762.]
- Heaviside, C., X.-M. Cai, and S. Vardoulakis, 2015: The effects of horizontal advection on the urban heat island in Birmingham and the West Midlands, United Kingdom during a heatwave. *Quart. J. Roy. Meteor. Soc.*, **141**, 1429–1441, doi:10.1002/qj.2452.
- Hempel, S., K. Frieler, L. Warszawski, J. Schewe, and F. Piontek, 2013: A trend-preserving bias correction—the ISI-MIP approach. *Earth Syst. Dyn.*, **4**, 219–236, doi:10.5194/esd-4-219-2013.
- Holt, D. W. E., 2015: Heat in US Prisons and Jails: Corrections and the Challenge of Climate Change. Sabin Center for Climate Change Law, Columbia Law School, 134 pp. [Available online at https://web.law.columbia.edu/sites/default/files/microsites/climate-change/holt_-_heat_in_us_prisons_and_jails.pdf.]
- Klinenberg, E., 2002: *Heat Wave: A Social Autopsy of Disaster in Chicago*. University of Chicago Press, 328 pp.

- Massey, N., and Coauthors, 2015: weather@home—development and validation of a very large ensemble modelling system for probabilistic event attribution. *Quart. J. Roy. Meteor. Soc.*, **141**, 1528–1545, doi:10.1002/qj.2455.
- Met Office, 2012: Met Office Integrated Data Archive System (MIDAS) Land and Marine Surface Stations Data (1853-current). NCAS British Atmospheric Data Centre, cited 2016. [Available online at <http://catalogue.ceda.ac.uk/uuid/220a65615218d5c9cc9e4785a3234bd0>.]
- Mitchell, D., and Coauthors, 2016a: Attributing human mortality during extreme heat waves to anthropogenic climate change. *Environ. Res. Lett.*, **11**, 074006, doi:10.1088/1748-9326/11/7/074006.
- , R. James, P. M. Forster, R. A. Betts, H. Shiogama, and M. Allen, 2016b: Realizing the impacts of a 1.5°C warmer world. *Nat. Climate Change*, **6**, 735–737, doi:10.1038/nclimate3055.
- Pal, J. S., and E. A. B. Eltahir, 2015: Future temperature in southwest Asia projected to exceed a threshold for human adaptability. *Nat. Climate Change*, **6**, 197–200, doi:10.1038/nclimate2833.
- Schaller, N., and Coauthors, 2016: Human influence on climate in the 2014 southern England winter floods and their impacts. *Nat. Climate Change*, **6**, 627–634, doi:10.1038/nclimate2927.
- Schleussner, C. F., J. F. Donges, R. V. Donner, and H. J. Schellnhuber, 2016: Armed-conflict risks enhanced by climate-related disasters in ethnically fractionalized countries. *Proc. Natl. Acad. Sci. USA*, **113**, 9216–9221, doi:10.1073/pnas.1601611113.
- Sippel, S., and F. E. L. Otto, 2014: Beyond climatological extremes – assessing how the odds of hydrometeorological extreme events in South-East Europe change in a warming climate. *Climatic Change*, **125**, 381–398, doi:10.1007/s10584-014-1153-9.
- Sonntag, D., 1990: Important new values of the physical constants of 1986, vapor pressure formulations based on the ITS-90, and psychrometer formulae. *Z. Meteorol.*, **70**, 340–344.
- Willett, K. M., and S. Sherwood, 2012: Exceedance of heat index thresholds for 15 regions under a warming climate using the wet-bulb globe temperature. *Int. J. Climatol.*, **32**, 161–177, doi:10.1002/joc.2257.